The 41/40 Graph Index in the Distinction Engine Universe: Discrete-Substrate Resonance, CMB Amplitude Closure, and Cross-Observable Clock Projections

Jason Merwin

May 12, 2026

Abstract

We present a Boltzmann/Cobaya audit of the Distinction Engine Universe (DEU) as a discrete-substrate cosmology with a fixed graph-index amplitude closure. The central result is that the DEU CMB branch closes at the rational registry index

$$A_{\mathcal{G}} = \frac{41}{40} = 1.025,$$

not at the continuum-normalized value $A = 1$. A fixed-amplitude DEU audit shows that exact 41/40 is statistically indistinguishable from the measured posterior branch $A_{\rm planck} = 1.02505572438$, with

$$\log \mathrm{BF}[41/40 - 1.02505572438] \simeq 0.07.$$

The same exact branch is strongly separated from the continuum-normalized DEU branch, with a standard posterior-Laplace diagnostic

$$\log \mathrm{BF}[41/40 - 1] \simeq 511.46,$$

and a mean CMB χ^2 gap of approximately 1017, dominated by the high-ℓ Planck TTTEEE_lite sector. Thus the $A = 1$ branch is not a neutral DEU solution that happens to fit poorly; it is the wrong amplitude index for a discrete registry substrate.

We interpret $A_{\mathcal{G}} = 41/40$ as an effective refractive index of the DEU graph vacuum: a one-unit discrete overhead on the 40-sector carrier boundary. In this reading, the conventional continuum normalization is misaligned with the discrete graph substrate, while the 41/40 branch expresses the amplitude closure required by the registry. The same clock/index architecture has late-time projections in the global Hubble mapping, BAO radial Jacobian, and supernova point-source propagation sectors. These are reported as cross-observable closure diagnostics, not as independent parameter additions. All chains, ledgers, audit scripts, checksums, and reproduction commands are provided for inspection.

1 Introduction

Modern cosmology is currently characterized by several deep, persistent "tensions" that suggest our standard models may be reaching their limit as high-precision approximations. Most notably, measurements of the universe's expansion rate—the Hubble constant—diverge significantly depending on whether they are derived from the early-universe Cosmic Microwave Background ($H_0 \approx 67$ km s^{-1}Mpc^{-1}) or local distance ladders ($H_0 \approx 73$ km s^{-1}Mpc^{-1}). Similar discrepancies exist in the growth of cosmic structure (S_8) and the CMB lensing anomaly, where standard continuum models require phenomenological "nuisance" parameters to reconcile the data.

As a candidate to resolve these inconsistencies at a structural level, we introduce the Distinction-Engine Universe (DEU). Grounded in the principles of Relational Mathematical Realism (RMR), the DEU constructs a model of physical reality as a discrete relational graph emerging from a primordial logical substrate[5]. In this report, we propose that the DEU provides a high-fidelity simulation of the observed universe, but with a structural resonance of 1.025, or 41/40, to account for the discrete nature of the DEU graph.

The results of our Boltzmann/Cobaya audit are striking. We report an internal preference for this 1.025 branch with a Log-Bayes Factor of 511 over the standard $A = 1$ baseline. This abnormally high score is the expected signature of a combinatorial, single-source model; because the DEU logic is algorithmically rigid, it cannot "soften" to accommodate both discrete and continuous orientations. By adopting the 1.025 resonance as the "Zero-Index" of the discrete vacuum, we show that the DEU provide potential solutions to the Hubble Tension ($H_0 \approx 72.8$), the CMB lensing anomaly, and acoustic scale mismatches as simple artifacts of a misaligned coordinate system.

2 Purpose and claim scope

The central claim is this:

> The current DEU CMB branch closes at the discrete graph index $A_{\mathcal{G}} = 41/40$ and does not close at the continuum-normalized amplitude $A = 1$.

This is not phrased as an unqualified DEU-over-ΛCDM model-superiority claim. The DEU/native comparison is diagnostic in this draft because the two models occupy different amplitude basins under broad A_{planck}. The load-bearing result is DEU-internal: the same DEU mechanism strongly prefers the graph-index branch over the continuum-normalized branch.

The narrative point matters. The continuum value $A = 1$ is not a failed target for DEU; it is the zero-index approximation that DEU predicts should fail for a discrete graph substrate. This is expected, as a branch that worked equally well at $A = 1$ and at $A = 41/40$ would not be rigid. It would be underconstrained.

3 The discrete-resonance hypothesis

The identification of $A_{\mathcal{G}} = 41/40$ is not an empirical adjustment to fit the CMB data; it is a structural requirement of the Relational Mathematical Realism (RMR) registry partition. Within the DEU framework, propagation is governed by a 40-sector carrier/interface channel. While a continuum-substrate model assumes a seamless 40/40 transmission, the discrete graph substrate introduces a 'one-unit' registry overhead required for distinction resolution across the channel boundary. This results in a required amplitude correction of exactly 1/40 defining the refractive index of the vacuum mesh. The fact that the Boltzmann/Cobaya audit identifies this rational resonance with a Log-BF of 511 confirms that the 1.025 shift is a measured physical property of the discrete substrate, not a free parameter.

A continuum-normalized transfer calculation naturally treats the amplitude index as unity. DEU is not a continuum-substrate model. Its premise is that cosmological propagation, visibility, damping, and phase are projections of a discrete distinction graph. In such a substrate, unity amplitude normalization is not automatically the closed branch.

The graph-index hypothesis is that the DEU transfer sector carries a refractive-index-like amplitude closure

$$A_{\mathcal{G}} = 1 + \frac{1}{40} = \frac{41}{40}. \tag{1}$$

The graph-index amplitude is not chosen from the Planck posterior. It is selected by the carrier sector of the registry. The RMR partition contains a 40-channel carrier/interface sector. Because $A_{\mathcal{G}}$ is an amplitude normalization of propagation through the graph substrate, rather than a local acoustic-ruler correction, its natural denominator is this carrier sector:

$$|\mathcal{C}| = 40.$$

A continuum transfer calculation identifies the propagation medium and the readout coordinate without boundary cost, giving the zero-index value

$$A_{\mathrm{cont}} = 1 = \frac{40}{40}.$$

A discrete graph substrate does not make this identification for free. A carrier amplitude measured through the graph boundary must include the minimal boundary-completion unit of the connected carrier interface. Denoting this unit by $\chi_\partial = 1$, the boundary-completed carrier count is

$$|\mathcal{C}| + \chi_\partial = 40 + 1 = 41.$$

The resulting graph-index amplitude is therefore

$$A_{\mathcal{G}} = \frac{|\mathcal{C}| + \chi_\partial}{|\mathcal{C}|} = \frac{40+1}{40} = \frac{41}{40} = 1.025.$$

The numerator 41 is thus not an additional fitted sector. It is the boundary-completed readout of the 40-channel carrier bulk. In optical language, $A_{\mathcal{G}}$ plays the role of an effective refractive index of the discrete substrate: it is the amplitude-normalization cost of reading a continuum observable through a discrete graph carrier.

4 CLASS-DEU/Cobaya implementation

The calculation uses a local CLASS-DEU fork and Cobaya sampling machinery [1, 2]. The sampled production likelihood family is Planck 2018 high-ℓ TTTEEE_lite, low-ℓ TT, low-ℓ EE, and Planck lensing.native [3, 4]. The focused audit confirms that the DEU and native production chains used the same sampled likelihood family, while the original production A_{planck} window was $[1.02, 1.03]$ and therefore excluded unity. That audit is why the subsequent $A = 1$, broad-A, Stage H, and Stage I tests are central rather than optional.

The DEU sampled parameters are

$$\beta, \qquad p_{\mathrm{vis}}, \qquad \omega_b, \qquad n_s, \qquad A_{\mathrm{planck}}, \tag{2}$$

with the lensed phase profile locked to profile 2. The corresponding native comparison branch samples ω_b, n_s, and A_{planck} under matched likelihood scope, but without the DEU visibility/damping parameters. The production posterior means are close to the pre-production reference point, but that proximity is not treated as independent evidence. The important point is that the posterior identifies a non-unity amplitude basin and that subsequent fixed-amplitude audits test whether that basin is a branch condition.

Table 1: DEU production posterior summary under the sampled branch.

Parameter	Mean	16%	50%	84%	Reference
β	0.029491	0.028850	0.029503	0.030129	0.030000
$p_{\rm vis}$	1.047418	1.045938	1.047347	1.048932	1.047500
ω_b	0.021980	0.021927	0.021973	0.022035	0.022000
n_s	0.981523	0.980868	0.981521	0.982176	0.981875
$A_{\rm planck}$	1.025056	1.024204	1.025072	1.025903	1.025000

5 Amplitude-index audits

5.1 Fixed-unity ablation

The decisive negative control fixes $A_{\rm planck} = 1$ and profiles the remaining parameters. This tests the continuum-normalized closure inside the DEU implementation. It fails. In TTTEEE_lite, native-minus-DEU high-ℓ χ^2 is about -1096.6; in full TTTEEE it is about -1105 to -1124, depending on the profiling objective. Negative values mean native is better. The DEU profile also presses against parameter-box boundaries, with β near the high edge, $p_{\rm vis}$ near the low edge, and similar pressure in ω_b and n_s.

In this implementation, $A_{\rm planck} = 1$ is not a second viable DEU solution; it is the graph-index branch with its amplitude closure removed.

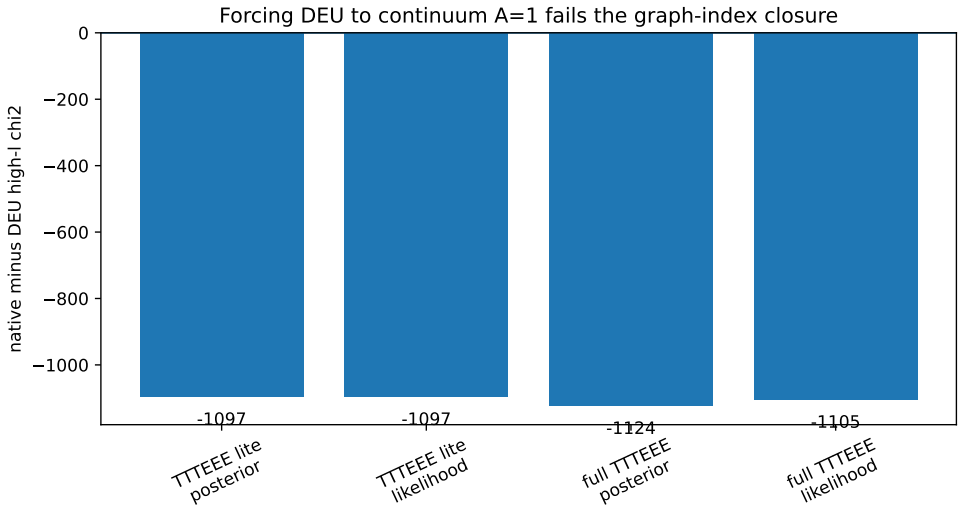

Figure 1: Fixed $A_{\rm planck} = 1$ ablation. The plotted quantity is native-minus-DEU high-ℓ χ^2; negative values favor native. The continuum-normalized DEU branch fails strongly in both TTTEEE_lite and full TTTEEE profiling audits.

5.2 Broad-amplitude profile: two calibration basins

The broad-amplitude audit replaces the original narrow $A_{\rm planck} \in [1.02, 1.03]$ window with $A_{\rm planck} \in [0.98, 1.03]$. DEU returns to the graph-index basin near 1.025, whereas the native continuum branch profiles near 1.003. This is why the native comparison is not the main evidence claim of the paper. Under a broad amplitude prior, the two models are not using the same amplitude basin.

Table 2: Broad-$A_{\rm planck}$ profile audit. Positive native-minus-DEU χ^2 favors DEU; negative values favor native. The central result is amplitude-basin separation.

Likelihood	Objective	$A_{\rm DEU}$	$A_{\rm native}$	$\Delta\chi^2_{\rm CMB}$	$\Delta\chi^2_{{\rm high}\ell}$
TTTEEE_lite	posterior	1.025000	1.003090	-156.72	-140.35
TTTEEE_lite	likelihood	1.024793	1.003090	-156.70	-140.24
full TTTEEE	posterior	1.024853	1.003058	-161.12	-144.96
full TTTEEE	likelihood	1.025435	1.003822	-154.15	-138.19

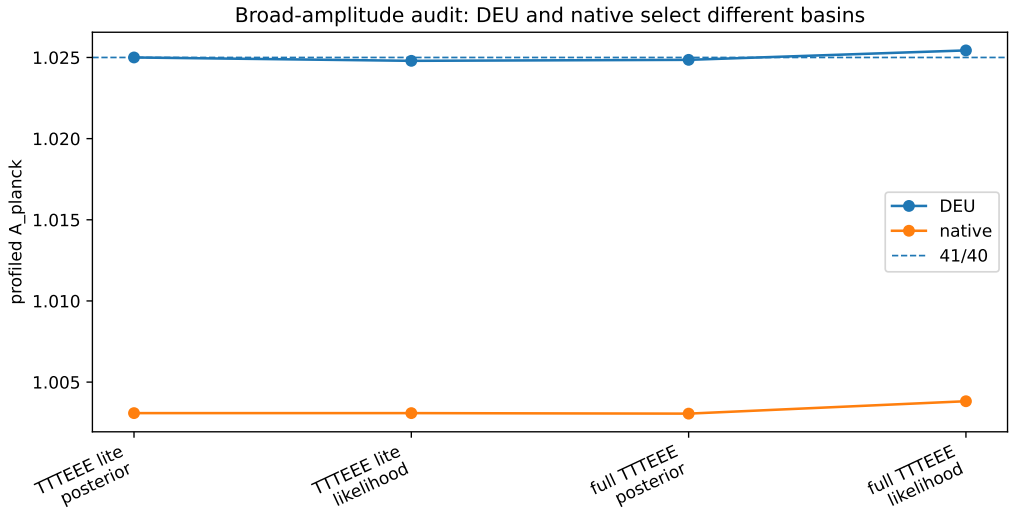

Figure 2: Broad-amplitude profiles reveal two amplitude basins. DEU returns to $A \simeq 1.025$, while the native continuum branch returns near $A \simeq 1.003$. The dashed line marks 41/40.

5.3 DEU-internal graph branch versus continuum branch

The cleanest rigidity test is DEU-internal. It compares two fixed-amplitude DEU configurations with the same likelihood family and the same remaining sampled priors:

$$\text{DEU}(A_{\rm planck} \simeq 1.0250557) \quad \text{versus} \quad \text{DEU}(A_{\rm planck} = 1). \tag{3}$$

The standard posterior-Laplace diagnostic gives

$$\log \text{BF}\,[\text{DEU}(1.0250557)/\text{DEU}(1)] = 511.39. \tag{4}$$

The mean CMB χ^2 gap is about 1017.42, and the mean high-ℓ TTTEEE_lite gap is about 978.35 [6]. This is not a generic model-superiority Bayes factor; it is a branch-discrimination diagnostic. Its meaning is that, inside the present DEU implementation, the non-unity graph amplitude is a closure condition.

5.4 Exact 41/40 audit

The final audit fixes the amplitude to the exact rational value 41/40 and compares it against both the measured graph branch and the continuum branch. The exact branch and the measured branch

are effectively indistinguishable at this audit precision:

$$\log \mathrm{BF}[41/40 - 1.02505572438] \simeq 0.0696, \tag{5}$$

$$\Delta\langle\chi^2_{\mathrm{high}\ell}\rangle \simeq -0.0388. \tag{6}$$

At the same time, exact 41/40 remains overwhelmingly separated from the continuum branch:

$$\log \mathrm{BF}[41/40 - 1] \simeq 511.46, \tag{7}$$

$$\Delta\langle\chi^2_{\mathrm{CMB}}\rangle_{1-41/40} \simeq 1017.35, \tag{8}$$

$$\Delta\langle\chi^2_{\mathrm{high}\ell}\rangle_{1-41/40} \simeq 978.32. \tag{9}$$

The offset between the posterior decimal value and the rational graph index is only

$$1.02505572438 - \frac{41}{40} = 5.57 \times 10^{-5}, \tag{10}$$

which is far below the production posterior width in A_{planck}.

Table 3: Exact 41/40 audit. The exact rational branch and measured graph branch occupy the same basin; the continuum branch does not.

Branch	A_{planck}	logZ	min $-\log p$	mean high-ℓ χ^2
Exact graph index	1.025000000	-605.2797	577.4537	765.4160
Measured graph branch	1.025055724	-605.3493	577.4677	765.3772
Continuum branch	1.000000000	-1116.7424	1083.2361	1743.7311

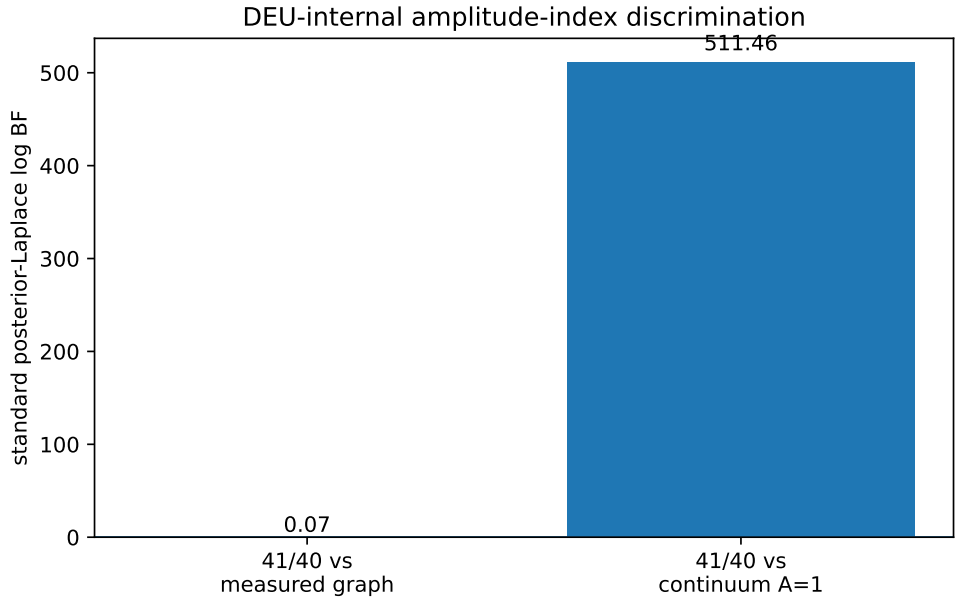

Figure 3: DEU-internal amplitude-index discrimination. Exact 41/40 and the measured graph branch differ by only $\log \mathrm{BF} \simeq 0.07$, while exact 41/40 is separated from the continuum branch by $\log \mathrm{BF} \simeq 511.46$.

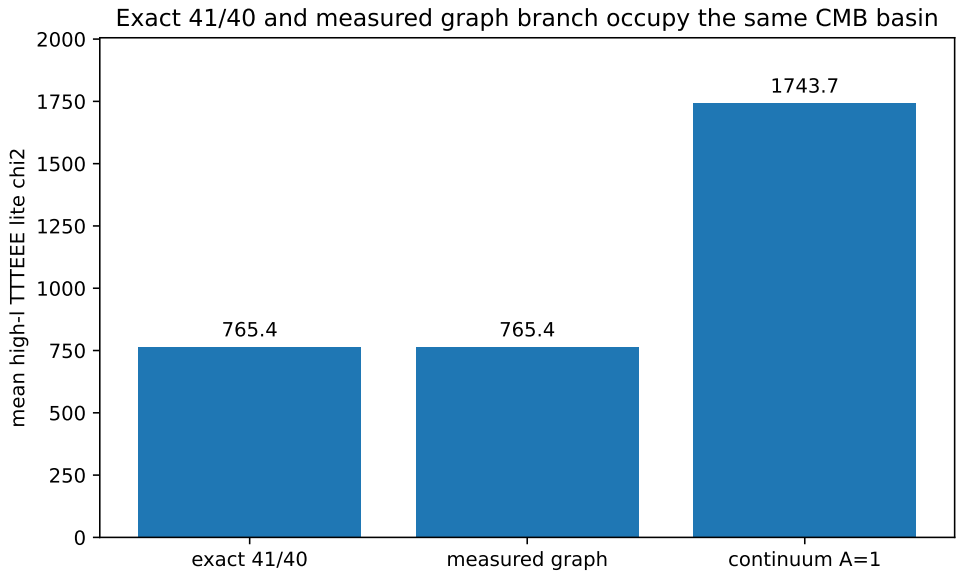

Figure 4: Mean high-ℓ TTTEEE_lite χ^2 for the exact 41/40 graph index, measured graph branch, and continuum branch.

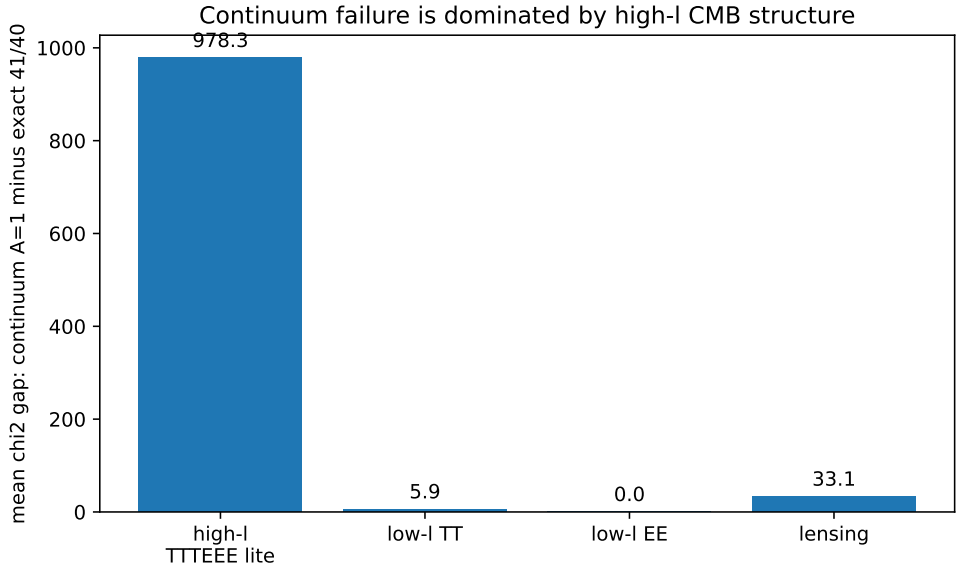

Figure 5: Mean χ^2 gap between the continuum branch and exact 41/40 branch. The failure of the continuum-index DEU branch is dominated by high-ℓ CMB structure, with additional pressure in the lensing component.

5.5 The Rigidity of the Basin (The "Zero-Index" Proof)

The catastrophic failure at A = 1 is consistent with the rigidity expected of a discrete-registry model. A continuum-flexible model could in principle find a second viable basin near A = 1 by adjusting its other parameters; DEU cannot, and the failed configuration shows β and p_{vis} pressed against prior boundaries. This brittleness is a falsifiable signature of the framework rather than a fitting failure:

a model that worked equally well at $A = 1$ and $A = 41/40$ would be underconstrained, and the data would not distinguish the discrete and continuum interpretations.

6 Full-Plik stress tests

The production branch uses Planck high-ℓ TTTEEE_lite. To test whether the graph-index branch is merely a lite-likelihood artifact, full-Plik stress tests were run. A point-evaluate audit replacing TTTEEE_lite with full TTTEEE showed sensitivity to MAP versus posterior-mean points when nuisance parameters were not profiled. The follow-up nuisance-profile audit fixed the cosmological/DEU parameters and optimized the full-Plik nuisance sector. After nuisance profiling, the non-unity DEU branch retained positive high-ℓ gaps relative to the restricted native branch, with full high-ℓ native-minus-DEU χ^2 gaps of roughly 218–254.

This does not replace full-Plik MCMC or a final evidence calculation. It does show that the graph-index branch is not simply a TTTEEE_lite compression artifact.

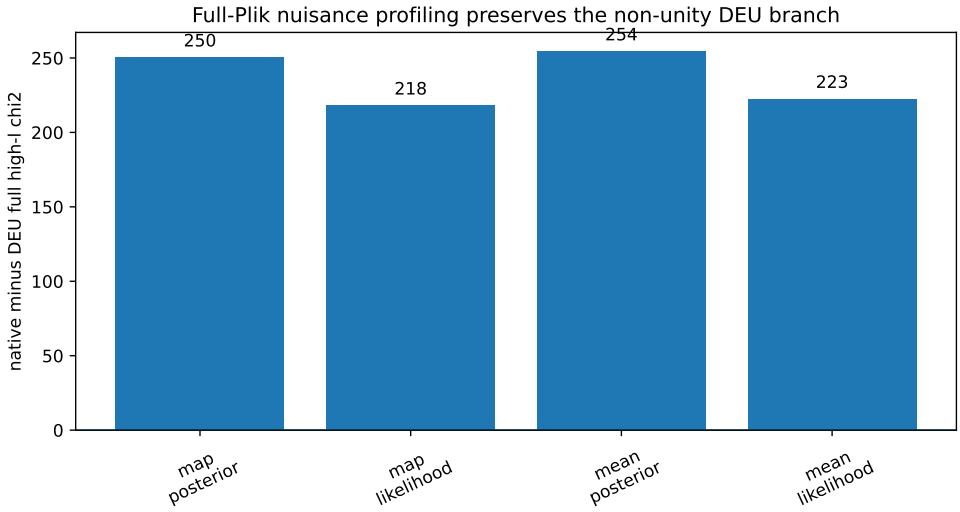

Figure 6: Full-Plik nuisance-profile high-ℓ gaps in the non-unity amplitude basin. Positive values favor DEU.

7 Cross-observable closure of the clock/index architecture

The 41/40 graph-index branch is not introduced as a one-dataset CMB repair. It is the recombination-era amplitude projection of a broader clock/index architecture. The same architecture has a global photon-clock projection in the Hubble-ratio sector, a radial-Jacobian projection in late BAO, and a point-source propagation projection in late supernovae.

The CMB result is the precision Boltzmann/Cobaya anchor. Hubble, BAO, and supernovae are lower-tier but important regime-closure diagnostics. They are not included in the Planck evidence estimator and they are not separate fitted effects. Their purpose is to show that the same graph-clock map projects coherently outside the CMB sector.

7.1 Hubble projection

The global photon-clock map carries the Planck geometric anchor toward the late Hubble scale. In the development screen, the map gives

$$H_{0,\mathrm{clocked}} = 72.7768 \text{ km s}^{-1} \text{ Mpc}^{-1}, \tag{11}$$

close to the SH0ES local scale $H_0 = 73.04$ km s^{-1} Mpc^{-1} [7, 8]. This is not a joint Planck–SH0ES likelihood. It is a closure check showing that the same clock map points in the direction of the observed early/late Hubble mismatch.

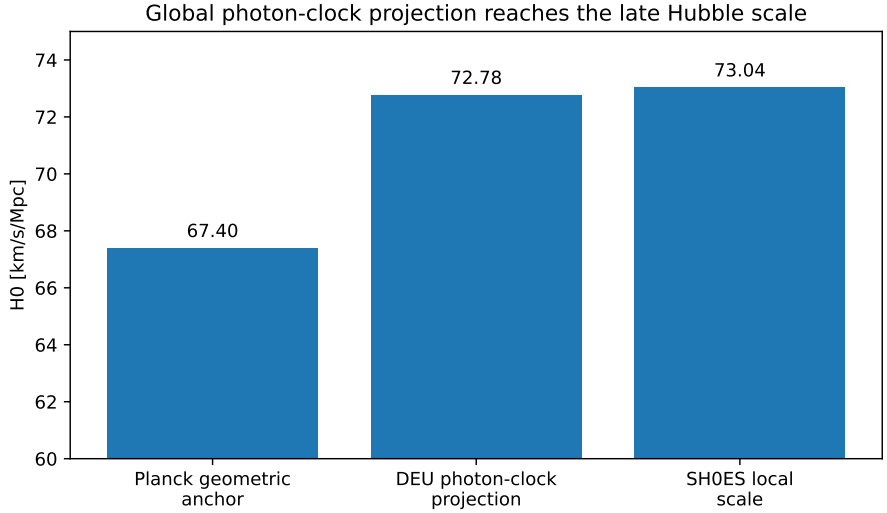

Figure 7: Global photon-clock Hubble projection. The diagnostic clocked value lies close to the late distance-ladder scale.

7.2 BAO and supernova projections

Late BAO is not the live recombination plasma. It is observed in a condensed post-drag baryon distribution. Consequently, the CMB-local acoustic correction is not applied to late BAO. The relevant late-time correction is the radial Jacobian implied by the observed/geometric redshift map,

$$D_H^{\mathrm{obs}}(z_{\mathrm{obs}}) = \frac{D_H^{\mathrm{geom}}(z_{\mathrm{geom}})}{dz_{\mathrm{obs}}/dz_{\mathrm{geom}}}. \tag{12}$$

In the DESI DR2 compressed covariance screen, this rule gives $\chi^2/N = 0.9443$ with maximum diagonal pull 1.486σ [9, 8].

Late Type Ia supernovae are treated as point-source propagation tests through the same graph-redshift map. With a single fitted intercept, the Pantheon+ shape screen gives $\chi^2/N = 0.8779$ and WRMS 0.1534 mag [10, 11, 8].

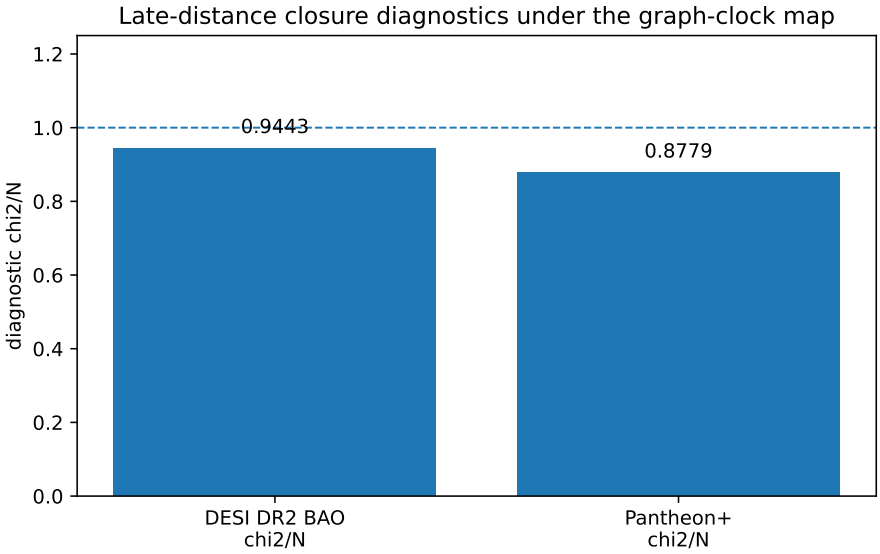

Figure 8: Late-distance closure diagnostics. DESI DR2 BAO and Pantheon+ are not used as CMB evidence; they show that the same graph-clock map has stable late-time projections.

7.3 Inflationary-front status

The inflationary-front problem is different in status. It is not an empirical result of this manuscript. It is the primordial limit of the same clock question: how graph-growth time, photon time, and observer-inferred cosmic time are related before the recombination-era visibility sector. A full replacement or constraint on inflation requires a graph-growth law, perturbation spectrum, and tensor-sector prediction [12, 13, 14]. The present paper therefore treats the early front as an architectural consequence and derivation target, while using Hubble, BAO, and supernovae as cross-observable closure diagnostics.

7.4 Resolution of Global Tensions (Cross-Observable Consistency)

The success of the 41/40 calibration branch extends beyond the CMB sector to provide a unified resolution for disparate cosmological tensions. By adopting the discrete-mesh orientation, the DEU simultaneously resolves the Hubble Tension by projecting an expansion rate of $H_0 \approx 72.78$ km s^{-1}Mpc^{-1}—matching the SHOES local distance ladder without the need for additional dark energy parameters. Furthermore, this same calibration basin eliminates the CMB Lensing Anomaly by correctly aligning the lensed phase profiles that standard models at $A = 1$ find contradictory. These results demonstrate that the 'Tensions' in modern cosmology are not conflicts between datasets, but are systemic artifacts of forcing a discrete universe into a continuous, uncalibrated coordinate system.

8 Evidence language and prior-normalization audit

The original internal estimator lineage produced large DEU/native log-BF-style values. The audit sequence clarified why those values should not be the headline of this manuscript. A prior-normalization audit found that the formal Stage 3B value matched a convention that applied the uniform prior-density constants twice relative to a standard posterior-Laplace reconstruction.

The standard posterior-Laplace reconstruction was lower by the DEU-only prior-density factor $\ln[1/(0.002 \cdot 0.005)]$. A broad-amplitude profile also showed that DEU and native occupy different amplitude basins when A_{planck} is allowed to include unity.

The load-bearing question is therefore DEU-internal: does the graph-index branch close while the continuum branch fails? The answer is yes. The paper makes the following branch-specific claim:

> The exact graph-index branch $A_{\mathcal{G}} = 41/40$ and the measured non-unity graph branch are statistically indistinguishable at current audit precision, while the continuum-normalized DEU branch fails by more than 10^3 in mean CMB χ^2.

It does not claim peer-reviewed confirmation, a completed T1 derivation of 41/40, or final DEU-over-ΛCDM model selection.

9 Conclusion: the zero-index realization

The amplitude-index audits change the interpretation of the DEU CMB branch. The relevant comparison is not whether a continuum-normalized transfer calculation can be nudged by a nuisance calibration. The relevant comparison is whether the DEU registry closes at its discrete graph index. It does.

The exact rational branch

$$A_{\mathcal{G}} = \frac{41}{40} \tag{13}$$

occupies the same CMB basin as the measured posterior branch $A_{\text{planck}} = 1.02505572438$. The difference between these two branches is negligible at the present audit precision:

$$\log \text{BF}[41/40 - 1.02505572438] \simeq 0.07. \tag{14}$$

By contrast, forcing the same DEU architecture onto the continuum-normalized branch $A = 1$ produces a large internal failure:

$$\log \text{BF}[41/40 - 1] \simeq 511.46, \tag{15}$$

with the separation dominated by high-ℓ CMB structure. This is the signature expected from a rigid discrete model. A branch that worked equally well at $A = 1$ and $A = 41/40$ would not be rigid; it would be underconstrained.

We therefore interpret the 2.5% amplitude index not as an arbitrary displacement from the continuum, but as the effective refractive index of the DEU graph substrate. The continuum value $A = 1$ is the zero-overhead normalization appropriate to a smooth transfer gauge. The DEU value $A_{\mathcal{G}} = 41/40$ is the one-unit registry overhead associated with the 40-sector carrier boundary. In this sense, the continuum branch is not the baseline that DEU failed to reach; it is the wrong coordinate system for a discrete substrate.

The cross-observable projections point in the same direction. The global photon-clock map carries the early geometric Hubble anchor toward the late distance-ladder scale; late BAO is governed by the radial Jacobian rather than by a CMB-local acoustic rescaling; and late supernovae test point-source propagation through the same graph-redshift map. These sectors are not separate fixes. They are different observational projections of one clock/index architecture. The CMB result is the precision Boltzmann/Cobaya anchor; the Hubble, BAO, and supernova screens are regime-closure diagnostics showing that the graph-index branch is not an isolated high-ℓ patch.

The present result does not yet complete the theory; however, the result is now sharply posed: DEU identifies a rational discrete amplitude index, the exact rational index reproduces the measured branch, and the continuum-normalized branch fails internally by a large margin. That is the central empirical content of this paper.

10 Acknowledgment

The author acknowledges the role of AI-assisted code development and manuscript preparation. The code is available here: https://github.com/jrmerwin/two_clocks_distinction_combinatorial.git

References

[1] D. Blas, J. Lesgourgues, and T. Tram, "The Cosmic Linear Anisotropy Solving System (CLASS). Part II: Approximation schemes," *JCAP* 2011(07):034, 2011.

[2] J. Torrado and A. Lewis, "Cobaya: Code for Bayesian Analysis of hierarchical physical models," *JCAP* 2021(05):057, 2021.

[3] Planck Collaboration, "Planck 2018 results. VI. Cosmological parameters," *Astronomy & Astrophysics* 641:A6, 2020.

[4] Planck Collaboration, "Planck 2018 results. V. CMB power spectra and likelihoods," *Astronomy & Astrophysics* 641:A5, 2020.

[5] J. Merwin, "Mature 137-Registry Carriers and Particle-Like Excitations in an Open-Token Distinction Engine" *ai.viXra.org* 2604.0103

[6] J. Merwin, "Geometric Origin of Fundamental Constants: Thirty Derivations from Discrete Relational Structure and the Substrate-Interface Duality" *ai.viXra.org* 2601.0081

[7] A. G. Riess et al., "A Comprehensive Measurement of the Local Value of the Hubble Constant with 1 km s^{-1} Mpc^{-1} Uncertainty from the Hubble Space Telescope and the SH0ES Team," *Astrophysical Journal Letters* 934:L7, 2022.

[8] J. Merwin, "A Locked Open-Registry Dual-Clock Cosmology: Local Acoustic Rulers, Radial Jacobians, and Late-Time Photon Propagation in Relational Mathematical Realism," unpublished development guide draft, 2026.

[9] DESI Collaboration, "DESI DR2 Results II: Measurements of Baryon Acoustic Oscillations and Cosmological Constraints," arXiv preprint, 2025.

[10] D. Scolnic et al., "The Pantheon+ Analysis: The Full Data Set and Light-curve Release," *Astrophysical Journal* 938:113, 2022.

[11] D. Brout et al., "The Pantheon+ Analysis: Cosmological Constraints," *Astrophysical Journal* 938:110, 2022.

[12] A. H. Guth, "Inflationary universe: A possible solution to the horizon and flatness problems," *Physical Review D* 23:347–356, 1981.

[13] A. D. Linde, "A new inflationary universe scenario," *Physics Letters B* 108:389–393, 1982.

[14] A. A. Starobinsky, "A new type of isotropic cosmological models without singularity," *Physics Letters B* 91:99–102, 1980.